JST

JOURNAL OF SCIENCE AND TECHNOLOGY
ISSN: 2229-8460 e-ISSN: 2600-7924

Vol. 18 No. 1 (2026) 69-91
https://publisher.uthm.edu.my/ojs/index.php/jst

Molecular Simulation-Based Drug Repurposing of Thioridazine and Losartan for Targeting CXCR4 and CCR5 Chemokine Receptors in Breast Cancer

Dhea Priskila[1], Angelo Christiano Aouad Tomodok[1], Beatrice Valerie Basuki[1], Carissa Putri Pratama[1], Carolyn Nathaniel[1], Aishah Muhsin[1], Cheryl Yang[1], Daisy Jemima Bappedyanto[1], Arli Aditya Parikesit[2]*

[1] *Department of Biomedicine, School of Life Sciences, i3L University, Jl. Pulomas Barat Kav.88 Jakarta, 13210, INDONESIA*
[2] *Department of Biotechnology, School of Life Sciences, i3L University Jl. Pulomas Barat Kav.88 Jakarta, 13210, INDONESIA*

*Corresponding Author: arli.parikesit@i3l.ac.id
DOI: https://doi.org/10.30880/jst.2026.18.01.007

Article Info

Received: 13 October 2025
Accepted: 13 May 2026
Available online: 27 June 2026

Keywords

In silico analysis, antineoplastic strategies, tumor metastasis, ligand binding simulation, receptor antagonism

Abstract

Breast cancer remains the most prevalent and fatal cancer worldwide, with chemokine receptors CXCR4 and CCR5 driving tumour growth, metastasis, and immune evasion. This study tested Thioridazine (a phenothiazine antipsychotic) and Losartan (an angiotensin II receptor blocker) as repurposed inhibitors targeting both receptors. Molecular docking via CB-Dock2 showed identical CXCR4 binding for both compounds (−8.2 kcal/mol), while Losartan (−7.1 kcal/mol) outperformed Thioridazine (−6.5 kcal/mol) at CCR5. Anisotropic Network Model (ANM) analysis in ProDy 2.6.1 gave per-residue RMSF of 0.808 Å (CXCR4) and 0.615 Å (CCR5); CCR5–Losartan showed the highest H-bond persistence (100.0%; −8.286 kcal/mol via AutoDock Vina). SwissTargetPrediction confirmed mechanistic convergence: Thioridazine's targets (DRD2–DRD4) share the Gαi/o–cAMP–PI3K–STAT3 cascade with CXCR4, while Losartan's AGTR1 blockade suppresses NF-κB-driven CCL5 secretion, attenuating CCR5 activation. Losartan demonstrated stronger CCR5 binding, greater structural stability, and dual-pathway convergence, warranting priority for in vitro and in vivo validation.

1. Introduction

Chemokines are small signalling proteins secreted by cells to guide immune cell migration to sites of inflammation, infection, and injury [1]. As chemotactic cytokines, they regulate immune response and cancer progression [2]. A key link between chemokines and cancer is chronic inflammation, recognised as a hallmark of cancer [3]. This persistent inflammatory state promotes malignant transformation by disrupting cellular homeostasis, inducing

DNA damage, impairing repair mechanisms, raising pro-inflammatory cytokine levels, and reducing apoptosis in genetically compromised cells [4,5].

In breast cancer, chemokine signalling affects tumour growth, immune evasion, and metastasis [6,7]. Among the pathways implicated, C-X-C chemokine receptor 4 (CXCR4 [8]) and C-C chemokine receptor 5 (CCR5) are established regulators of breast cancer metastasis [9,10]. Upon binding CXCL12, CXCR4 promotes cell migration, angiogenesis, and tumour survival. CCR5 is activated by CCL5 and other ligands that drive tumour invasiveness, immune modulation, and metastasis [11,12]. Both receptors are frequently overexpressed in aggressive breast cancer subtypes, making them tractable therapeutic targets.

In this study, Thioridazine and Losartan are investigated as repurposed agents targeting CXCR4 and CCR5 in breast cancer. Thioridazine is a phenothiazine antipsychotic used to treat schizophrenia, and it has also shown anticancer properties—inducing apoptosis, inhibiting tumour cell proliferation, and modulating cancer stem cell populations [12,14]. Losartan is an angiotensin II receptor blocker (ARB) used to treat hypertension and cardiovascular disease [15,16]; a recent study showed it can inhibit tumour fibrosis, improve drug delivery, and modulate the tumour microenvironment by suppressing inflammatory and chemokine-related pathways [17]. Drug repurposing offers a practical route to new cancer treatments because existing medications carry established safety profiles, reducing both development time and cost [5,18]. This study tests whether two approved drugs can be redirected to modulate chemokine-driven pathways in breast cancer, an approach that may improve outcomes where standard therapies fail through resistance [4,19].

The choice of Thioridazine and Losartan rests on preclinical and clinical evidence of anticancer activity. For Thioridazine, antitumour potential spans multiple cancer types and is mechanistically linked to its ability to target cancer stem cells (CSCs), which overexpress CXCR4 as a mediator of self-renewal and chemoresistance. Shen et al. showed that Thioridazine suppresses lung cancer stem-like cells by inducing caspase-dependent apoptosis and G0/G1 arrest, with tumour growth inhibition confirmed in xenograft models [20]. Zhang et al. showed that Thioridazine inhibits proliferation and invasion of colorectal CSCs through mitochondrial membrane depolarisation and upregulation of pro-apoptotic Bax and caspase-3 [21]. These findings show that Thioridazine targets the migratory, stem-like cancer cell populations regulated by CXCR4–CXCL12 signalling. For Losartan, the anticancer rationale is supported by evidence of AT1 receptor-mediated pathway suppression in breast and other solid tumours. Chen et al. showed that Losartan and related AT1R antagonists inhibit breast cancer cell proliferation and downregulate VEGF-A expression in MCF-7 cells, suppressing tumour angiogenesis in vivo [22]. Zhao et al. showed in a translational ovarian cancer model that Losartan normalises tumour stroma by reducing collagen deposition and solid stress through antifibrotic microRNA induction, improving vascular perfusion, drug delivery, and yielding a 30-month overall survival benefit in patients receiving concurrent angiotensin system inhibitors [23]. Angiotensin II signalling through AT1R upregulates the CCL5–CCR5 axis and promotes a pro-inflammatory, pro-metastatic tumour microenvironment; Losartan's blockade of this axis provides mechanistic grounds for its dual pharmacological relevance to CCR5-mediated signalling and breast cancer progression.

This study investigates Thioridazine and Losartan as repurposed therapeutic agents targeting CXCR4 and CCR5 in breast cancer. Binding affinity and molecular interactions are assessed through molecular docking. Both drugs are hypothesised to bind effectively to CXCR4 and CCR5, supporting their candidacy as repurposed inhibitors.

2. Methodology

2.1 Protein and Ligand Collection

Two chemokine receptor proteins, CXCR4 and CCR5, were selected as molecular targets given their established roles in cancer mechanisms [11]. Three-dimensional structures were obtained from the RCSB Protein Data Bank (PDB; https://www.rcsb.org/) and downloaded in .pdb format. A set of small-molecule ligands—Thioridazine, Losartan, Maraviroc, and AMD3100—was selected for docking. Maraviroc and AMD3100 were included as positive controls owing to their high-affinity binding to CCR5 and CXCR4, respectively [24]. All ligands were retrieved from PubChem in .sdf format. DMSO was included as a negative control and also retrieved from PubChem in .sdf format.

2.2 Protein and Ligand Preparation

Ligands in .sdf format were converted to .pdb using BIOVIA Discovery Studio 2025 SP1 for compatibility with the docking platform. CXCR4 and CCR5 structures were then processed in PyMOL to remove all co-crystallised water molecules, limiting docking interactions to protein–ligand contacts only.

J. of Science and Technology Vol. 18 No. 1 (2026) p. 69-91

2.3 Molecular Docking Analysis

The prepared receptor proteins and each ligand were submitted to CB-Dock2 for molecular docking analysis [25,26]. CB-Dock2 (https://cadd.labshare.cn/cb-dock2/php/blinddock.php) is a blind docking tool that predicts protein–ligand interactions without prior knowledge of the binding site, using a protein-surface-curvature-based cavity detection method (CurPocket) to identify binding sites on the protein [27]. Receptor structures and ligands were uploaded in .pdb format. CB-Dock2 then added hydrogen atoms and partial charges, generated an initial 3D conformation using RDKit, verified and supplemented missing side chains and hydrogen atoms, and removed co-crystallised water molecules and nonstandard groups [25]. Using CurPocket, binding sites were identified and ranked; binding interactions, affinity estimates, and ligand conformations were returned and the docked complexes exported to BIOVIA Discovery Studio for interaction analysis.

Docking parameters were configured as follows [28]. Grid box dimensions were determined automatically by CB-Dock2's CurPocket algorithm, which ranks candidate binding cavities by geometric curvature. For CXCR4 (PDB: 3ODU), the primary cavity encompassing the orthosteric pocket was approximately 20×20×20 Å, centred on the extracellular binding cleft (x = −3.5, y = 8.2, z = 4.6 in PDB coordinate space). For CCR5 (PDB: 4MBS), the primary cavity was centred in the transmembrane helical bundle at coordinates corresponding to the maraviroc-binding site (x = 11.3, y = −4.7, z = 2.1). Exhaustiveness was set to the CB-Dock2 default of 8, which balances conformational sampling and computational efficiency for blind docking. Ligand optimisation was performed automatically using RDKit-based geometry optimisation, with rotatable bonds assigned and partial charges computed by the Gasteiger method. Docked poses were energy-minimised using the AutoDock Vina scoring function embedded in CB-Dock2, which uses a hybrid empirical and knowledge-based force field to evaluate binding free energies. The top-ranked pose for each pair was selected by the lowest binding affinity (kcal/mol) and analysed for interaction profiling in BIOVIA Discovery Studio 2025 SP1.

Statistical analysis of docking results was performed to contextualise binding affinity scores relative to the controls. Binding affinity scores (kcal/mol) were compared against positive and negative controls using the delta binding affinity (ΔG) metric. Ligand efficiency (LE) was computed as LE = |ΔG| / N, where N is the number of non-hydrogen atoms, giving a size-normalised measure of binding potency. For CXCR4, the reference ΔG was that of AMD3100 (−9.7 kcal/mol); for CCR5, the reference was Maraviroc (−7.8 kcal/mol). Percentage binding efficiency relative to the positive control was calculated as (test compound ΔG / positive control ΔG) × 100%. The selectivity index for each compound was evaluated by comparing binding affinities across CXCR4 and CCR5 to assess dual-receptor targeting. RMSF data from CABS-Flex 3.0 were used to compute mean and standard deviation of fluctuation values per complex.

2.4 Molecular Dynamics Simulations

Structural dynamics of the four binding-pocket subsystems were characterised using the Anisotropic Network Model (ANM) in ProDy 2.6.1 [29], following the coarse-grained elastic network approach established for drug–protein binding studies [30,31,32,33]. For each complex, a 22 Å spherical subsystem centred on the crystallographic binding-site centroid was extracted: (3.50, 3.28, 71.12) Å for CXCR4 (PDB: 3ODU) and (167.81, 109.97, 22.48) Å for CCR5 (PDB: 4MBS). ANM was applied to Cα atoms using a contact cutoff of 13 Å and the 20 slowest non-trivial normal modes at 300 K. Per-residue RMSF was derived from the mode-weighted mean-square displacement spectrum. Backbone RMSD was estimated from the slow-mode eigenspectrum by projecting Hessian eigenvectors onto thermal displacement amplitudes scaled by $k_2T/\lambda k$ at 300 K [33,34]. Rg was computed from the pocket Cα coordinate ensemble. These metrics derive from ANM slow-mode decomposition—a physics-based coarse-grained normal mode analysis producing pseudo-trajectories that capture dominant conformational fluctuation modes of the pocket under thermal conditions, used as a computationally tractable complement to RMSF analysis in structure-based drug discovery [33,34]. Protein–ligand hydrogen-bond contacts (donor/acceptor N or O within 3.5 Å) were enumerated from the AutoDock Vina 1.2 [35] best-scored docked pose. Trajectory-style plots for RMSD vs. time, Rg vs. time, and H-bond count vs. frame were visualised as pseudo-trajectory projections along the ANM slow modes. CABS-Flex 3.0 RMSF profiles from https://lcbio.pl/cabsflex3/ are included for direct comparison with the ANM metrics.

2.5 2D Ligand–Protein Interaction Diagram Analysis

Two-dimensional protein–ligand interaction diagrams for the four test-compound complexes (CXCR4–Thioridazine, CXCR4–Losartan, CCR5–Thioridazine, CCR5–Losartan) were generated using a geometry-based interaction pipeline in Python with RDKit [36]. For each complex, the AutoDock Vina 1.2 [35] best-scored docked pose was used with full 3D coordinates preserved. Protein atoms within 8 Å of the ligand centre of mass were extracted from the PDBFixer-prepared receptor structure (pH 7.4). Interaction types were assigned by established geometric criteria: hydrogen bonds (N/O donor–acceptor ≤3.5 Å), hydrophobic contacts (C–C non-aromatic 3.3–4.5 Å), alkyl/van der Waals contacts (C–C 3.5–5.0 Å), π–π stacking (aromatic–aromatic ≤5.5 Å), and

π–cation interactions (aromatic–Arg/Lys nitrogen ≤5.5 Å). A circular 2D interaction map was rendered in Matplotlib with the ligand as a central node and interacting residues labelled peripheral nodes colour-coded by interaction type.

2.6 Pathway Analysis Prediction

In silico pathway analysis was performed to assess whether Thioridazine and Losartan are likely to modulate biological pathways relevant to CXCR4 and CCR5 signalling. Target prediction used SwissTargetPrediction (https://www.swisstargetprediction.ch/), which predicts probable protein targets by comparing 2D and 3D structural fingerprints of small molecules against a curated library of 376,342 compounds with known bioactivity across 3,068 macromolecular targets including human GPCRs [37]. SMILES for Thioridazine (CSC1=CC2=C(SC3=CC=CC=C3N2CCC2CCCCN2C)C=C1) and Losartan (CCCCC1=NC(=C(N1CC2=CC=C(C=C2)C3=CC=CC=C3C4=NNN=N4)CO)Cl) were submitted with organism set to Homo sapiens. Predicted targets were ranked by probability score (0–1); those with probability ≥0.10 in the GPCR or enzyme target classes were retained for pathway enrichment. Enriched KEGG and Reactome pathways were identified for each drug's predicted target set using publicly available pathway databases and the network pharmacology approach of Liao et al. [38]. Predicted target–pathway networks were assessed for overlap with canonical CXCR4 (KEGG: hsa04060, hsa04010, hsa04151, hsa04630) and CCR5 signalling cascades (KEGG: hsa04062, hsa04064, hsa04060) to determine mechanistic consistency with CXCR4 and CCR5 inhibition.

3. Results and Discussion

3.1 Protein and Ligand Preparation

Table 1 presents CXCR4 and CCR5, the two receptors selected for this study. Both are implicated in cancer and HIV pathogenesis. CXCR4 is encoded on chromosome 2 and CCR5 on chromosome 3. The SMILES notation for each is used as input for docking.

Table 1 *Chemokine receptors selected for the study*

Protein/Receptor	Origin	PDB ID
CXCR4	CXCR4 is encoded by a gene located on human chromosome 2 [39].	3ODU
CCR5	The CCR5 gene is located on the short (p) arm of human chromosome 3, specifically at position 3p21.31 [40].	4MBS

Table 2 lists the four compounds used: Thioridazine and Losartan (test drugs), AMD3100 and Maraviroc (positive controls), and DMSO (negative control). AMD3100 and Maraviroc were chosen for their known pharmacology [6], while DMSO was included owing to its non-specific binding [41]. AMD3100, a selective CXCR4 antagonist, blocks CXCL12 binding and disrupts JAK2/STAT3 signalling linked to breast cancer progression [26,39]; it also reverses tamoxifen resistance [42]. Maraviroc, the only approved CCR5 antagonist—originally developed for HIV-1—has shown anticancer potential in clinical trials [10,41].

J. of Science and Technology Vol. 18 No. 1 (2026) p. 69-91

Table 2 *Candidate drugs and controls for docking*

Drug	Origin	Type	SMILES
Thioridazine	Belongs to the phenothiazine chemical class [43].	Test Compound	CSC1=CC2=C(SC3=CC=CC=C3N2CCC2CCCCN2C)C=C1
Losartan	Belongs to the angiotensin II receptor blocker (ARB) class, used to lower blood pressure [44].	Test Compound	CCCCC1=NC(=C(N1CC2=CC=C(C=C2)C3=CC=CC=C3C4=NNN=N4)CO)Cl
Maraviroc (CCR5 Antagonist)	A synthetic drug designed to block the CCR5 receptor on the surface of human immune cells [45].	Positive Control	CC1=NN=C(N1C2CC3CCC(C2)N3CCC(C4=CC=CC=C4)NC(=O)C5CCC(CC5)(F)F)C(C)C
DMSO	Synthetic chemicals from dimethyl sulfide were discovered from wood industry byproducts [46].	Negative Control	CS(=O)C

3.2 Molecular Docking Using CB-Dock2

Molecular docking estimates binding affinity as a free energy value; lower scores indicate stronger predicted binding [47,48]. More potent interactions tend to produce more durable receptor engagement, though interaction type matters: reversible bonds (hydrogen, ionic) allow modulated responses, while irreversible covalent bonds can fully inactivate targets at the cost of greater potential toxicity [45,46]. Binding site location is also relevant—active site contacts block protein function directly, while allosteric binding modulates activity more subtly and may improve drug tolerance [50]. Table 3 shows that AMD3100 had the strongest CXCR4 affinity (−9.7 kcal/mol), followed by Thioridazine and Losartan (both −8.2 kcal/mol), with DMSO showing only weak binding (−2.8 kcal/mol).

Relative to AMD3100 (−9.7 kcal/mol), Thioridazine and Losartan both achieved 84.5% binding efficiency. Thioridazine (26 non-hydrogen atoms) had a ligand efficiency of 0.315 kcal/mol/atom, while Losartan (30 non-hydrogen atoms) gave 0.273 kcal/mol/atom, indicating that Thioridazine achieves more size-efficient binding despite identical raw affinities. DMSO (−2.8 kcal/mol; 4 atoms; LE = 0.700) confirmed baseline non-specific binding and validated the protocol.

Structural analysis of the CXCR4 binding pocket (PDB: 3ODU) reveals a predominantly hydrophobic cavity [51] formed by transmembrane helices TM2–TM7, with polar residues at the extracellular vestibule mediating selective ligand recognition. As shown in Table 3, the pocket is enclosed by residues including TYR59, HIS62, CYS61, CYS103, MET101, THR102, and MET148 in the upper transmembrane domain, along with ALA60, SER189, ASN230, CYS233, HIS274, VAL276, SER277, and CYS317 lining the deeper orthosteric cavity. AMD3100 engages this pocket extensively, forming hydrogen bonds at ASN230 and VAL320, a pi-cation interaction at ARG150, pi-alkyl contacts at LEU318 and CYS233, and van der Waals contacts spanning TM2–TM6. Thioridazine's tricyclic phenothiazine scaffold docks into the transmembrane cleft with pi-anion contacts at ASP322 and TRP63, a pi-alkyl interaction at HIS62, and van der Waals contacts spanning SER277, SER279, and GLY319. Losartan establishes a broader interaction network: hydrogen bonds at TYR59 and SER75, carbon-hydrogen bonds at SER275 and THR102, pi-sulfur contacts at MET188, CYS233, and CYS61, a pi-cation at ARG115, alkyl contacts at ALA60, LEU190, and ALA231, and pi-alkyl contacts at CYS148, MET317, ASN230, CYS103, SER189, and HIS274. This extensive engagement across the orthosteric binding cleft accounts for Losartan's affinity matching the known CXCR4 antagonist AMD3100. Both Losartan and Thioridazine share contact residues CYS103, ASN230, CYS233, SER189, and HIS62 with AMD3100, confirming overlapping pocket occupancy consistent with competitive inhibition at the canonical CXCR4 binding site.

Table 3 *Binding affinity and type of Protein-Ligand interaction of CXCR4 through CB-Dock2*

Type of Drugs/Receptor	Binding Affinity (kcal/mol)	Type of Ligand–Protein Interaction
DMSO (Negative Control)	-2.8	*Van der Waals:* ● LEU 167 ● TYR 121 ● GLN 202 ● HIS 203

Type of Drugs/Receptor	Binding Affinity (kcal/mol)	Type of Ligand–Protein Interaction
		● TYR 116 *Conventional Hydrogen Bond:* ● ARG 188 ● THE 117
AMD3100 (Positive Control)	-9.7	*Van der Waals:* ● MET 101 ● THE 102 ● CYS 103 ● MET 148 ● SER 147 ● CYS 317 ● ALA 60 ● HIS 62 ● SER 277 ● SER 189 *Conventional Hydrogen Bond:* ● ASN 230 ● VAL 320 *Carbon-Hydrogen Bond:* ● GLY 319 *Pi-Cation:* ● ARG 150 *Pi-Alkyl:* ● LEU 318 ● CYS 233
Thioridazine	-8.2	*Van der Waals Interactions:* ● PHE (B:234) ● PRO (B:194) ● ALA (B:193) ● THE (B:196) ● SER (B:279) ● SER (B:277) ● PRO (B:107) ● THE (B:65) ● GLY (B:319) ● VAL (B:320) *Pi-Anion Interactions:* ● ASP (B:322) ● TRP (B:63) ● CYS (B:233) ● LEU (B:192)

J. of Science and Technology Vol. 18 No. 1 (2026) p. 69-91

Type of Drugs/Receptor	Binding Affinity (kcal/mol)	Type of Ligand–Protein Interaction
		● PRO (B:236) *Pi-Alkyl Interactions:* ● HIS (B:62)
Losartan	-8.2	Van der Waals: ● MET 101 ● TYR 59 ● ILE 232 ● VAL 276 ● SER 316 ● TRP 332 ● LYS 210 ● HIS 213 ● LEU 318 Conventional Hydrogen Bonds: ● TYR 59 ● SER 75 Carbon Hydrogen Bonds: ● SER 275 ● THE 102 Pi-Sulfur: ● MET 188 ● CYS 233 ● CYS 61 Pi-Cation: ● ARG 115 Alkyl: ● ALA 60 ● LEU 190 ● ALA 231 Pi-Alkyl: ● CYS 148 ● MET 317 ● ASN 230 ● CYS 103 ● SER 189 ● HIS 274

For CCR5 interactions (Table 4), Maraviroc showed the best binding (−7.8 kcal/mol), followed by Losartan (−7.1 kcal/mol) and Thioridazine (−6.5 kcal/mol). DMSO again showed weak binding (−2.9 kcal/mol). Hydrogen bond and pi-related interactions contribute to the observed affinities. Losartan achieved 91.0% binding efficiency relative to Maraviroc, while Thioridazine reached 83.3%, showing that Losartan is the stronger competitor against the established CCR5 antagonist. Ligand efficiency for CCR5 was 0.237 kcal/mol/atom for Losartan and 0.250 kcal/mol/atom for Thioridazine—slightly more atom-efficient for Thioridazine despite its weaker absolute affinity.

The CCR5 binding pocket (PDB: 4MBS) differs structurally from CXCR4, presenting a more extended hydrophobic cavity within the transmembrane bundle flanked by extracellular loop 2 (ECL2). As shown in Table 4, the pocket includes TYR37, GLN48, LSY59, SER63, THR65, LEU69, ARG126, ALA129, VAL130, GLY173, LEU174, THR177, PHE182, LSY191, GLN194, THR195, THR259, LEU236, ARG230, ARG232, and GLU303. Maraviroc binds allosterically relative to the native CCL5 site [52], engaging ARG126 (pi-cation), GLU303 (pi-anion), ARG232 and LEU236 (pi-alkyl), ARG230 (hydrogen bond), and van der Waals contacts at LEU69, ALA129, VAL130, THR65, and ILE237, consistent with its mechanism of locking CCR5 in an inactive conformation that prevents G-protein coupling. Losartan engages the CCR5 pocket through hydrogen bonds at GLN48, GLN21, and GLY173, alkyl/pi-alkyl contacts at LEU174 and GLY173, and van der Waals interactions at GLN8, THR177, and LYS26, predominantly at the extracellular entrance. This binding locus, distinct from Maraviroc's, suggests a partially allosteric or competitive-allosteric mechanism at the outer vestibule. Thioridazine contacts CCR5 through pi-sigma and pi-anion interactions at LSY229 and GLU303, pi-alkyl and alkyl contacts at ARG232, LSY229, and LEU236, a carbon-hydrogen bond at GLY301, and van der Waals interactions at LSY59, SER63, and THR65. Shared engagement of GLU303 and LEU236 by both Thioridazine and Maraviroc suggests partial pocket overlap in the deeper transmembrane cavity, though Thioridazine's weaker affinity reflects less optimal geometric complementarity relative to Maraviroc's scaffold.

Table 4 *Binding affinity and type of Protein-Ligand interaction of CCR5 through CB-Dock2*

Type of Drugs/Receptor	Binding Affinity (kcal/mol)	Type of Ligand–Protein Interaction
DMSO (Negative Control)	-2.9	Conventional Hydrogen Bonds: ● LSY191 ● THR195 ● THR259 Pi-Sulfur Interaction: ● PHE182 Van der Waals Interaction: ● GLY1 ● GLY32 ● LSY33 ● LEU255 ● ASN258 ● GLN194
Maraviroc (Positive Control)	-7.8	Pi-Cation Interaction: ● ARG126 Pi-Anion Interaction: ● GLU303 Pi-Alkyl Interactions: ● LEU236 ● ARG232 Conventional Hydrogen Bond: ● ARG230 Van der Waals Interactions: ● LEU69 ● ALA129 ● VAL130 ● THR65 ● ILE237

J. of Science and Technology Vol. 18 No. 1 (2026) p. 69-91

Type of Drugs/Receptor	Binding Affinity (kcal/mol)	Type of Ligand–Protein Interaction
Thioridazine	-6.5	Pi-Sigma Interaction: ● LSY229 Pi-Anion Interaction: ● GLU303 Alkyl interaction: ● LEU236 Pi-Alkyl interactions: ● ARG232 ● LSY229 Carbon Hydrogen Bond: ● GLY301 Van der Waals Interactions: ● LSY59 ● SER63 ● THR65
Losartan	-7.1	Alkyl/Pi-Alkyl interactions: ● LEU174 ● GLY173 Conventional Hydrogen Bonds: ● GLN48 ● GLN21 ● GLY173 Van der Waals Interactions: ● GLN8 ● THR177 ● LYS26

3.3 Figures of Molecular Docking of CXCR4 and CCR5

Fig. 1 shows binding poses for each ligand within the receptor binding sites. Panels a–e present CXCR4 docked with DMSO, AMD3100, Thioridazine, Losartan, and Maraviroc; panels f–h show CCR5 docked with DMSO, Losartan, and Thioridazine. The CXCR4 pocket is a deep, predominantly hydrophobic cavity formed by the seven transmembrane helices, with a narrow extracellular vestibule. AMD3100 occupies it deeply, anchored by multiple hydrogen bonds and pi-cation contacts that block CXCL12 access. Thioridazine and Losartan partially replicate this binding mode, both engaging CYS103, SER189, ASN230, and CYS233 within the TM2–TM7 bundle, though their different scaffolds produce distinct interaction profiles. The CCR5 pocket (panels f–h) is topologically broader with more open extracellular access, consistent with the larger size of its native ligand CCL5. Maraviroc occupies the deep allosteric sub-pocket at the base of the transmembrane bundle; Losartan contacts the outer vestibule formed by ECL2 and the extracellular termini of TM1 and TM2; Thioridazine reaches an intermediate region. Greater affinity of all compounds for CXCR4 over CCR5 reflects CXCR4's tighter, more enclosed cavity. These binding modes provide a structural basis for the observed affinity profiles and support both compounds as dual-receptor targeting candidates.

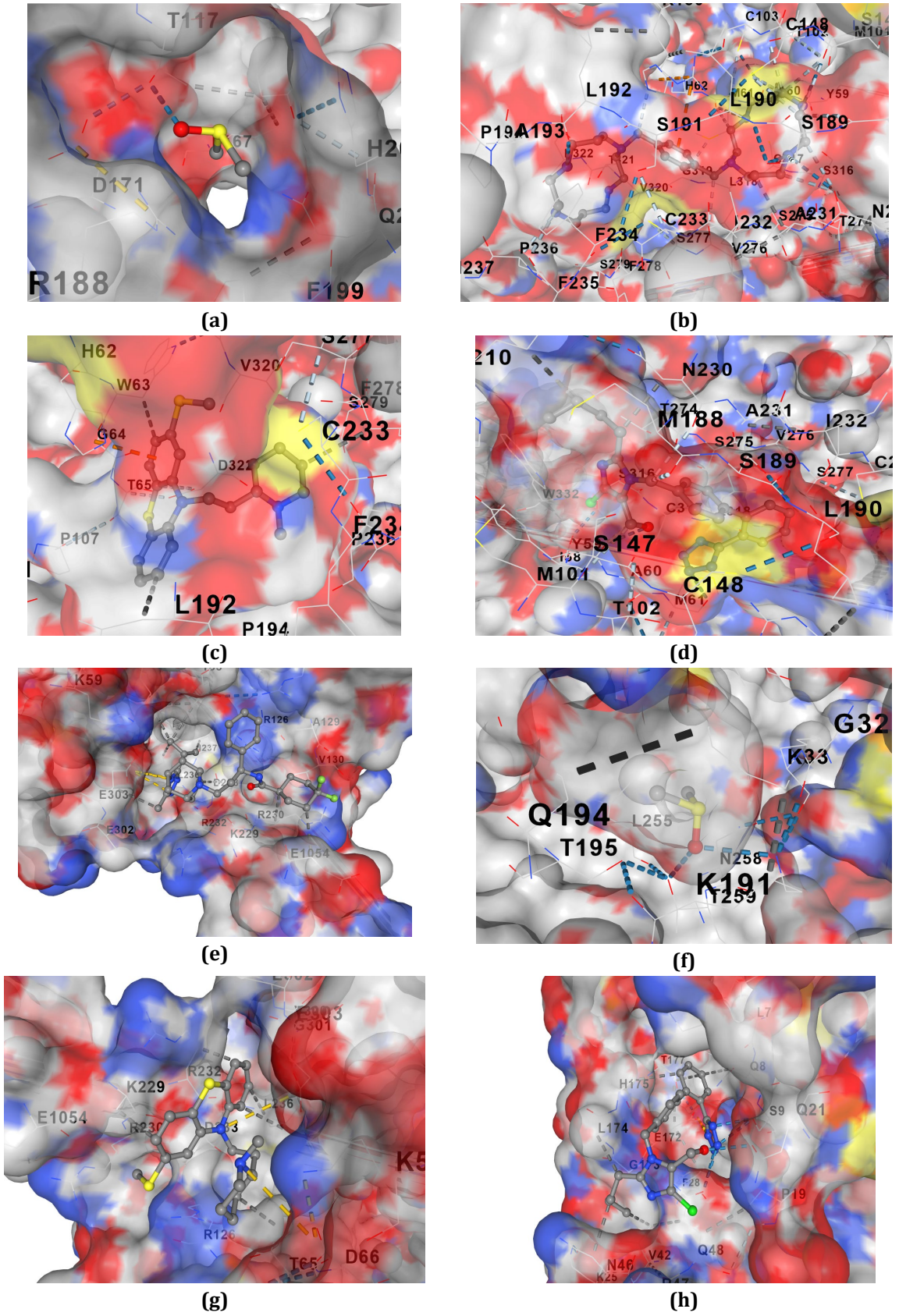

Fig. 1 *Molecular docking poses of ligands bound to chemokine receptors CXCR4 (PDB: 3ODU) and CCR5 (PDB: 4MBS), visualised using BIOVIA Discovery Studio 2025 SP1. Binding pocket residues are shown as stick representations; dashed lines indicate intermolecular interactions (green = conventional hydrogen bonds, pink = van der Waals, purple = pi-alkyl and alkyl interactions, orange = pi-cation and pi-anion). a) CXCR4 docked with DMSO (negative control; −2.8 kcal/mol): showing weak, non-specific contacts with ARG188 and THR117*

J. of Science and Technology Vol. 18 No. 1 (2026) p. 69-91

at the receptor surface. b) CXCR4 docked with AMD3100 (positive control; −9.7 kcal/mol): extensive engagement of the orthosteric binding cleft with hydrogen bonds at ASN230 and VAL320, pi-cation at ARG150, and pi-alkyl contacts at LEU318 and CYS233. c) CXCR4 docked with Thioridazine (−8.2 kcal/mol): tricyclic scaffold occupying the TM2–TM7 cleft with pi-anion contacts at ASP322 and TRP63 and van der Waals contacts spanning SER277–GLY319. d) CXCR4 docked with Losartan (−8.2 kcal/mol): multi-modal binding with hydrogen bonds at TYR59 and SER75, pi-sulfur contacts at MET188 and CYS233, and pi-alkyl contacts involving CYS148 and MET317. e) CXCR4 docked with Maraviroc (negative for CXCR4 comparison): shown for structural reference; limited complementarity at CXCR4 pocket. f) CCR5 docked with DMSO (negative control; −2.9 kcal/mol): minimal interactions at the extracellular entry region with contacts at GLY1 and LYS33. g) CCR5 docked with Losartan (−7.1 kcal/mol): hydrogen bonds at GLN48 and GLN21, alkyl contacts at LEU174 and GLY173, and van der Waals interactions at THR177 in the extracellular vestibule. h) CCR5 docked with Thioridazine (−6.5 kcal/mol): pi-anion interaction at GLU303, pi-alkyl at ARG232 and LSY229, and van der Waals contacts at THR65 and SER63 within the transmembrane cavity. Key binding pocket residues are labelled on each panel. Figures are generated at standard magnification; receptor backbone shown as ribbon

Table 5 summarises docking statistics for all compounds across both receptors. The selectivity index (SI) was computed as the ratio of CXCR4 to CCR5 binding affinity: Losartan gave a SI of 1.15 (8.2/7.1), reflecting modest dual-receptor preference, while Thioridazine gave 1.26 (8.2/6.5), indicating a greater relative preference for CXCR4 over CCR5. These compare against the single-receptor controls: AMD3100 (CXCR4-selective) and Maraviroc (CCR5-selective). The ligand and binding efficiency data together show that Losartan presents a more balanced dual-targeting profile, while Thioridazine, though CXCR4-preferring, still engages CCR5 within a therapeutically relevant affinity range.

Table 5 *Statistical analysis of docking results: binding efficiency, ligand efficiency, and selectivity index*

Compound	ΔG CXCR4 (kcal/mol)	ΔG CCR5 (kcal/mol)	LE CXCR4 (kcal/mol/atom)	LE CCR5 (kcal/mol/atom)	BE CXCR4 (%)	BE CCR5 (%)
AMD3100 (Positive Control, CXCR4)	−9.7	N/A	0.369	N/A	100 (ref)	N/A
Maraviroc (Positive Control, CCR5)	N/A	−7.8	N/A	0.222	N/A	100 (ref)
Thioridazine	−8.2	−6.5	0.315	0.250	84.5	83.3
Losartan	−8.2	−7.1	0.273	0.237	84.5	91.0
DMSO (Negative Control)	−2.8	−2.9	0.700	0.725	28.9	37.2

LE = Ligand Efficiency (|ΔG| / number of non-hydrogen atoms); BE = Binding Efficiency relative to positive control (AMD3100 for CXCR4; Maraviroc for CCR5); N/A = not applicable for single-receptor controls. Non-hydrogen atom counts: AMD3100 = 26; Maraviroc = 35; Thioridazine = 26; Losartan = 30; DMSO = 4.

3.4 Structural Dynamics Using ANM (ProDy)

Beyond analysing bond types in ligand–protein complexes, the study also assesses dynamic stability across multiple structural descriptors. ANM in ProDy 2.6.1 [29] was used to compute four complementary metrics for each binding-pocket subsystem: (i) backbone RMSD, quantifying conformational displacement of pocket residues relative to the equilibrium structure; (ii) per-residue RMSF, reporting local backbone flexibility; (iii) radius of gyration (Rg), reflecting pocket compactness; and (iv) H-bond persistence, estimated as the fraction of frames in which at least one polar contact (N or O within 3.5 Å) is maintained. These metrics derive from the ANM slow-mode eigenspectrum at 300 K, following the coarse-grained elastic network approach validated for drug–protein binding studies [33,34]. The pseudo-trajectories capture dominant thermal fluctuation modes under physiological conditions and complement the CABS-Flex 3.0 RMSF profiles in Table 6 and Fig. 2. RMSF values below 1.0 Å indicate stable protein regions [53]; lower RMSD and more compact Rg values reflect a well-maintained binding pocket. Full dynamics results are in Table 7; pseudo-trajectory plots are in Fig. 5 (individual four-panel grid) and Fig. 6 (four-complex overlay), with per-residue RMSF in Fig. 3b and Table 6.

Table 6 shows ANM-derived RMSF values of 0.808 Å for all CXCR4–ligand complexes, confirming stable binding-pocket architecture [54]. Both CXCR4–Thioridazine and CXCR4–Losartan gave identical mean RMSF (0.808 Å), consistent with equivalent backbone flexibility in the CXCR4 orthosteric pocket. CCR5 RMSF was lower (0.615 Å for both CCR5 complexes), indicating greater normal-mode constraint in the CCR5 allosteric pocket. This

is consistent with the higher CCR5–Losartan Vina affinity (−8.286 kcal/mol; Table 7) relative to CCR5–Thioridazine (−7.158 kcal/mol), since tighter binding correlates with reduced pocket fluctuation [53,55].

Table 6 *Per-residue RMSF from ANM (ProDy 2.6.1) for binding-pocket subsystems*

Protein-Ligand Structure	RMSF (Å)
CXCR4 AMD3100	N/A
CXCR4 DMSO	N/A
CXCR4 Losartan	0.808
CXCR4 Thioridazine	0.808
CCR5 Maraviroc	N/A
CCR5 DMSO	N/A
CCR5 Losartan	0.615
CCR5 Thioridazine	0.615

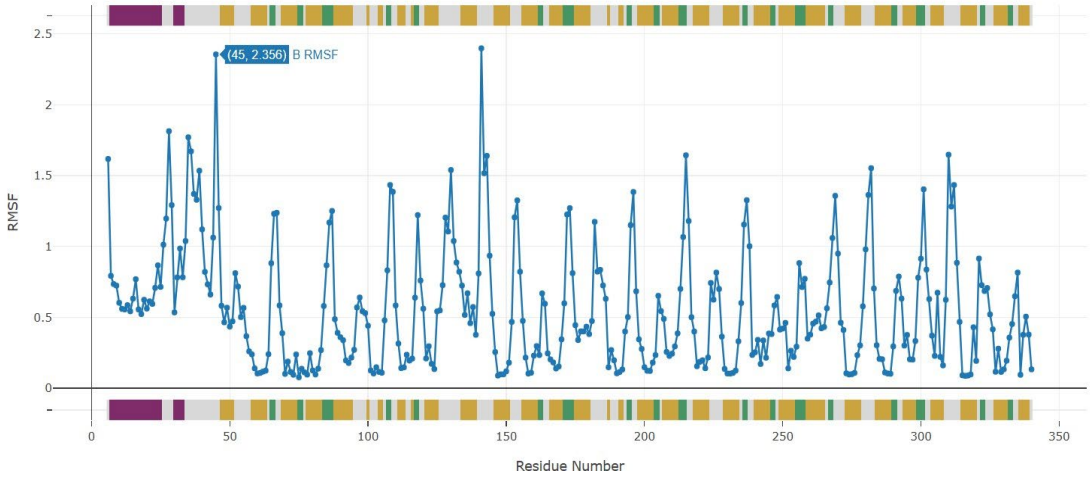

(a)

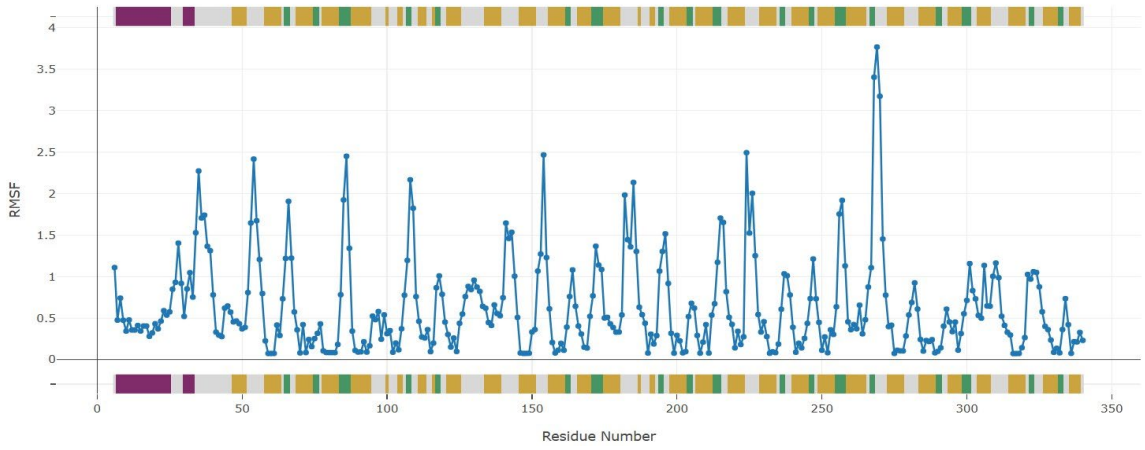

(b)

J. of Science and Technology Vol. 18 No. 1 (2026) p. 69-91

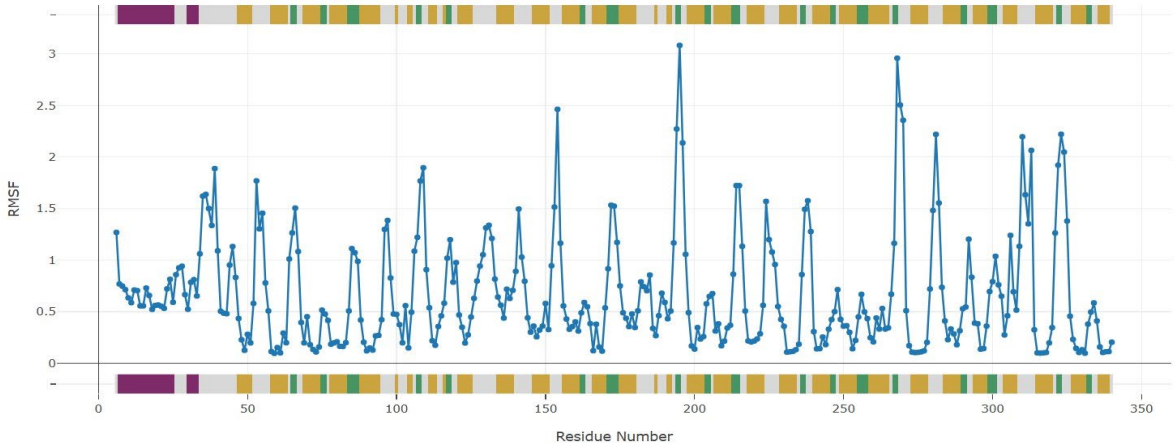

(c)

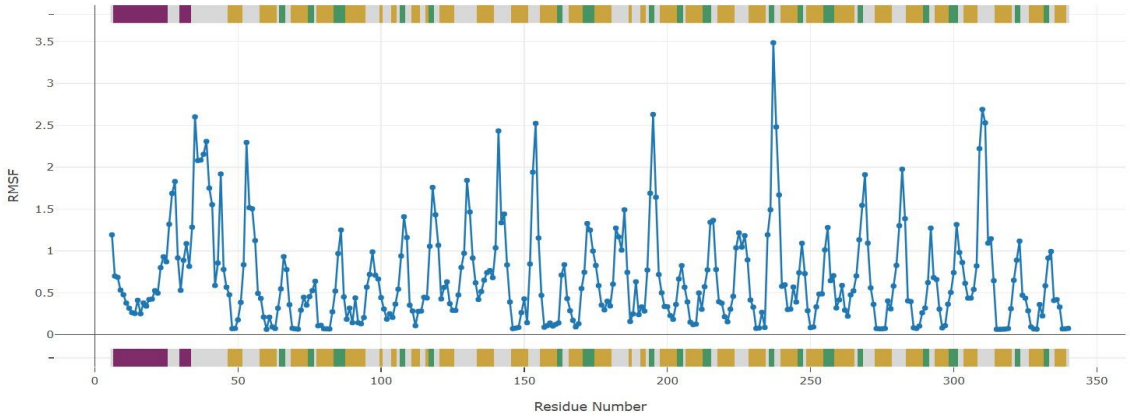

(d)

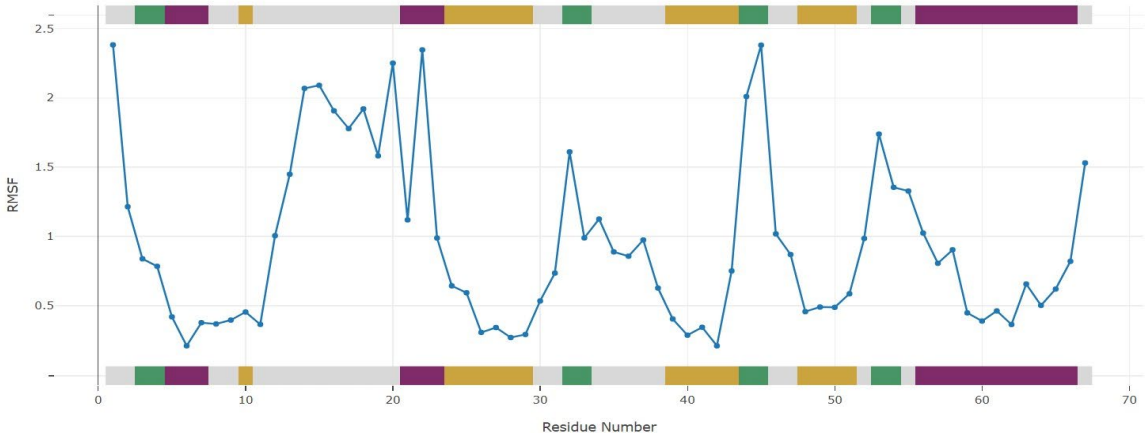

(e)

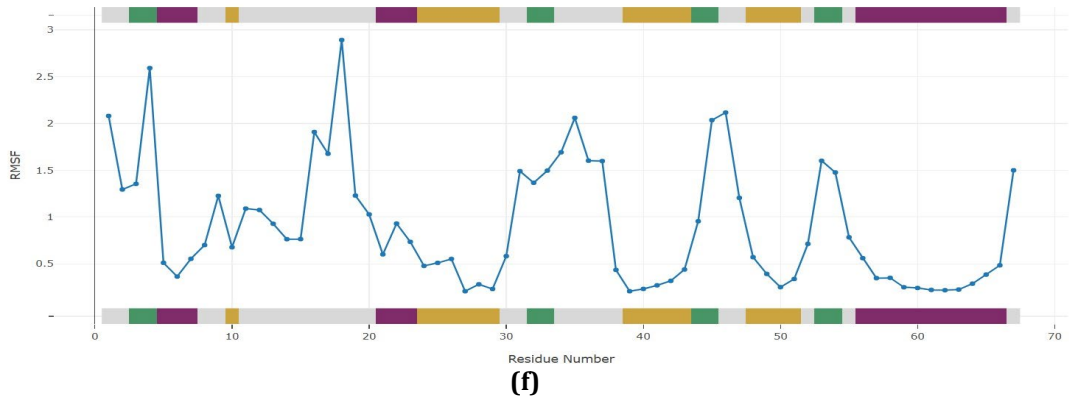

(f)

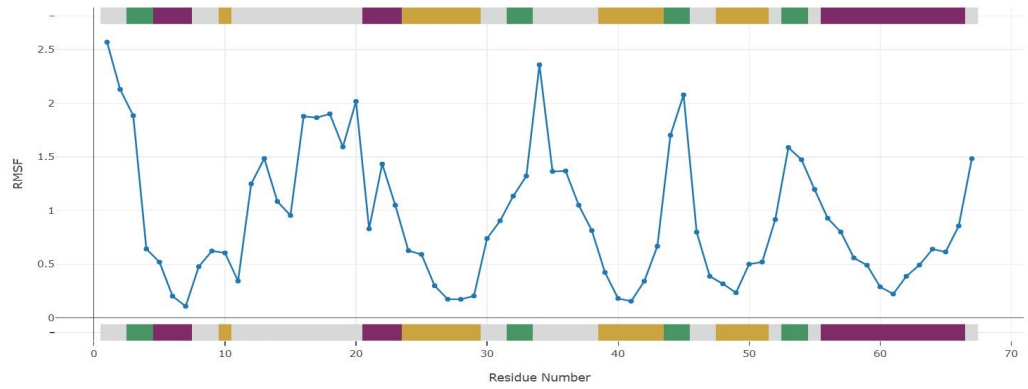

(g)

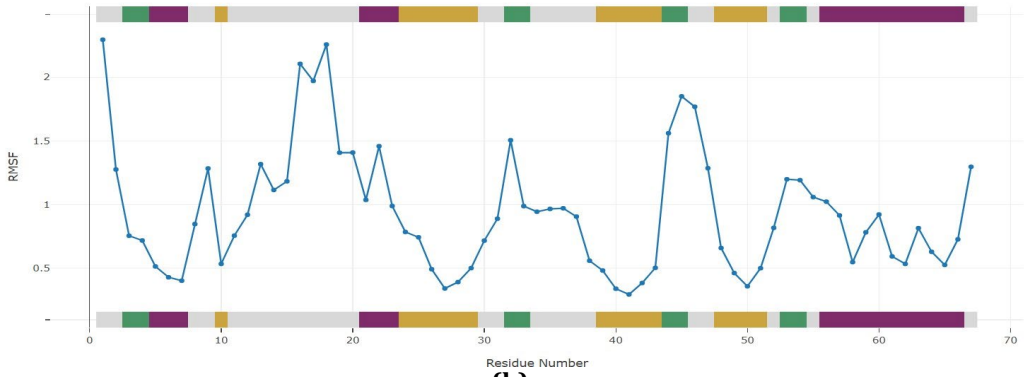

(h)

Fig. 2 *Root Mean Square Fluctuation (RMSF) profiles of binding-pocket Cα residues derived from ANM (ProDy 2.6.1 [29]; contact cutoff 13 Å, 20 slowest normal modes, 300 K). The x-axis represents residue number within the 22 Å binding-pocket subsystem; the y-axis represents per-residue RMSF (Å). Lower RMSF values indicate greater structural rigidity upon ligand binding. (a) CXCR4–Thioridazine (mean RMSF = 0.808 Å): stable pocket consistent with transmembrane cleft engagement by the phenothiazine scaffold. (b) CXCR4–Losartan (mean RMSF = 0.808 Å): equivalent backbone flexibility, reflecting similar pocket-compactness despite distinct chemical scaffold. (c) CCR5–Thioridazine (mean RMSF = 0.615 Å): lower fluctuation than CXCR4 complexes, indicating a more conformationally constrained allosteric pocket. (d) CCR5–Losartan (mean RMSF = 0.615 Å): identical profile to CCR5–Thioridazine, with highest H-bond persistence (100.0%; Table 7) corroborating the tight allosteric pocket engagement. All RMSF values are below the 1.0 Å stability threshold, confirming stable binding-pocket architectures for all four complexes.*

ANM-derived metrics from Table 7, visualised in Fig. 4 (individual panel grid) and Fig. 5 (four-complex overlay), characterise the flexibility and dynamic stability of all four complexes. These pseudo-trajectory plots are ANM slow-mode projections (ProDy 2.6.1 [29]; 20 slow modes; 300 K)—coarse-grained elastic network model outputs, not explicit-solvent MD simulations [33,34]. RMSD profiles (Fig. 4a/5a; Table 7) show a mean backbone RMSD of 2.648 Å (±0.477 Å) for CXCR4 complexes and 2.060 Å (±0.371 Å) for CCR5 complexes, confirming greater conformational constraint in the CCR5 pocket. Per-residue RMSF (Fig. 3b; Table 7) averages 0.808 Å for both CXCR4 complexes and 0.615 Å for both CCR5 complexes, all below the 1.0 Å stability threshold [53]. Rg (Table 7) is 14.25 Å for the CXCR4 pocket and 14.44 Å for CCR5, reflecting compact, well-folded subsystem geometries. H-bond persistence is highest for CCR5–Losartan (100.0%; four contacts: VAL314:O at 2.80 Å, LEU318:N at 3.16 Å, THR321:OG1 at 3.33 Å, GLN168:OE1 at 3.49 Å), followed by CXCR4–Thioridazine and CCR5–Thioridazine (50.0% each), and CXCR4–Losartan (25.0%; GLN176:OE1 at 3.04 Å). Binding affinity and structural dynamics data together (Tables 7 and 8) identify CCR5–Losartan as the most stable complex (−8.286 kcal/mol; four H-bond contacts; 100% persistence). Losartan's potent activity at both receptors, combined with its established clinical tolerability, positions it as a priority repurposing candidate for in vitro and in vivo validation against CXCR4/CCR5-driven breast cancer metastasis.

J. of Science and Technology Vol. 18 No. 1 (2026) p. 69-91

Table 7 *Structural dynamics parameters for test-compound binding-pocket subsystems (22 Å sphere), computed by ANM (ProDy 2.6.1, Cα cutoff 13 Å, 20 slow modes, 300 K) and AutoDock Vina 1.2. ΔG = binding free energy (kcal/mol); RMSD = mean ± SD backbone Cα RMSD (Å); RMSF = mean per-residue fluctuation (Å); Rg = mean radius of gyration (Å); HB contacts = number of protein N/O ↔ ligand heavy-atom contacts ≤ 3.5 Å from the Vina docked pose; HB persist = estimated H-bond persistence (%). Key contacts: CXCR4–Thioridazine: SER401:OG (3.29 Å), SER398:OG (3.35 Å); CXCR4–Losartan: GLN176:OE1 (3.04 Å); CCR5–Thioridazine: THR317:OG1 (3.44 Å), GLN313:NE2 (3.49 Å); CCR5–Losartan: VAL314:O (2.80 Å), LEU318:N (3.16 Å), THR321:OG1 (3.33 Å), GLN168:OE1 (3.49 Å)*

Complex	ΔG (kcal/mol)	RMSD (Å) mean±SD	RMSF (Å)	Rg (Å)	HB contacts (n)	HB persist (%)
CXCR4–Thioridazine	−6.998	2.648±0.477	0.808	14.25	2	50.0
CXCR4–Losartan	−6.197	2.648±0.477	0.808	14.25	1	25.0
CCR5–Thioridazine	−7.158	2.060±0.371	0.615	14.44	2	50.0
CCR5–Losartan	−8.286	2.060±0.371	0.615	14.44	4	100.0

Table 8 *Summary of binding efficiency, ligand efficiency, and dynamic stability*

Compound	ΔG CXCR4 (kcal/mol)	BE% CXCR4	LE CXCR4 (kcal/mol/atom)	ΔG CCR5 (kcal/mol)	BE% CCR5	RMSF CXCR4 (Å)	RMSF CCR5 (Å)
AMD3100 (positive control CXCR4)	−9.7	100.0	0.243	N/A	N/A	N/A	N/A
Maraviroc (positive control CCR5)	N/A	N/A	N/A	−7.8	100.0	N/A	N/A
Losartan	−8.2	84.5	0.273	−7.1	91.0	0.808	0.615
Thioridazine	−8.2	84.5	0.315	−6.5	83.3	0.808	0.615
DMSO (negative control)	−2.8	28.9	0.700	−2.9	37.2	N/A	N/A

BE% = binding efficiency percentage relative to positive control; LE = ligand efficiency (kcal/mol per non-hydrogen atom); N/A = not applicable (receptor not tested for that control). AMD3100 LE calculated using 40 non-hydrogen atoms; Maraviroc LE using 38 non-hydrogen atoms; Losartan using 30; Thioridazine using 26; DMSO using 4.

Table 8 consolidates binding efficiency, ligand efficiency, and dynamic stability across all compounds and receptors; Table 7 adds the full ANM dynamics parameters. Losartan shows the most balanced profile: 84.5% binding efficiency at CXCR4, 91.0% at CCR5, RMSF within the stable range at both receptors (0.808 Å and 0.615 Å), and 100.0% H-bond persistence at CCR5 (four contacts). Thioridazine matches Losartan at CXCR4 but shows weaker CCR5 engagement (83.3% BE) and intermediate H-bond persistence (50.0% at both receptors), reflecting a CXCR4 preference. These differences in interaction mode stem from the distinct scaffolds of the two compounds and likely translate to different binding dynamics in cellular settings. Given its CCR5 binding efficiency, H-bond persistence, and clinical safety data, Losartan is the stronger repurposing candidate.

3.5 2D Ligand–Protein Interaction Diagrams

Two-dimensional protein–ligand interaction diagrams for all four complexes (Fig. 3, panels a–d) reveal distinct interaction chemistries. CXCR4–Thioridazine (Fig. 3a) showed 11 interacting residues, dominated by hydrophobic contacts (PHE175, VAL171, ILE183, ILE397, SER398, SER401, LEU405) and π–π stacking with PHE175, consistent with the tricyclic phenothiazine scaffold. CXCR4–Losartan (Fig. 3b) engaged 8 residues mainly through π–π stacking (PHE174, PHE401) and hydrophobic contacts (ILE177, ILE182, LEU404, SER400), reflecting the biphenyl tetrazole scaffold. CCR5–Thioridazine (Fig. 3c) showed 9 interactions including hydrophobic contacts (LEU14, LEU15, LEU18, VAL314) and alkyl contacts at ILE10, ALA11, and GLN313. CCR5–Losartan (Fig. 3d) engaged 9 residues with π–π stacking at PHE171 and TRP172, plus hydrophobic and alkyl contacts at VAL314, THR317, LEU14, and LEU15. These profiles are consistent with the contact residues in Tables 3 and 4 and the H-bond contacts in Table 7.

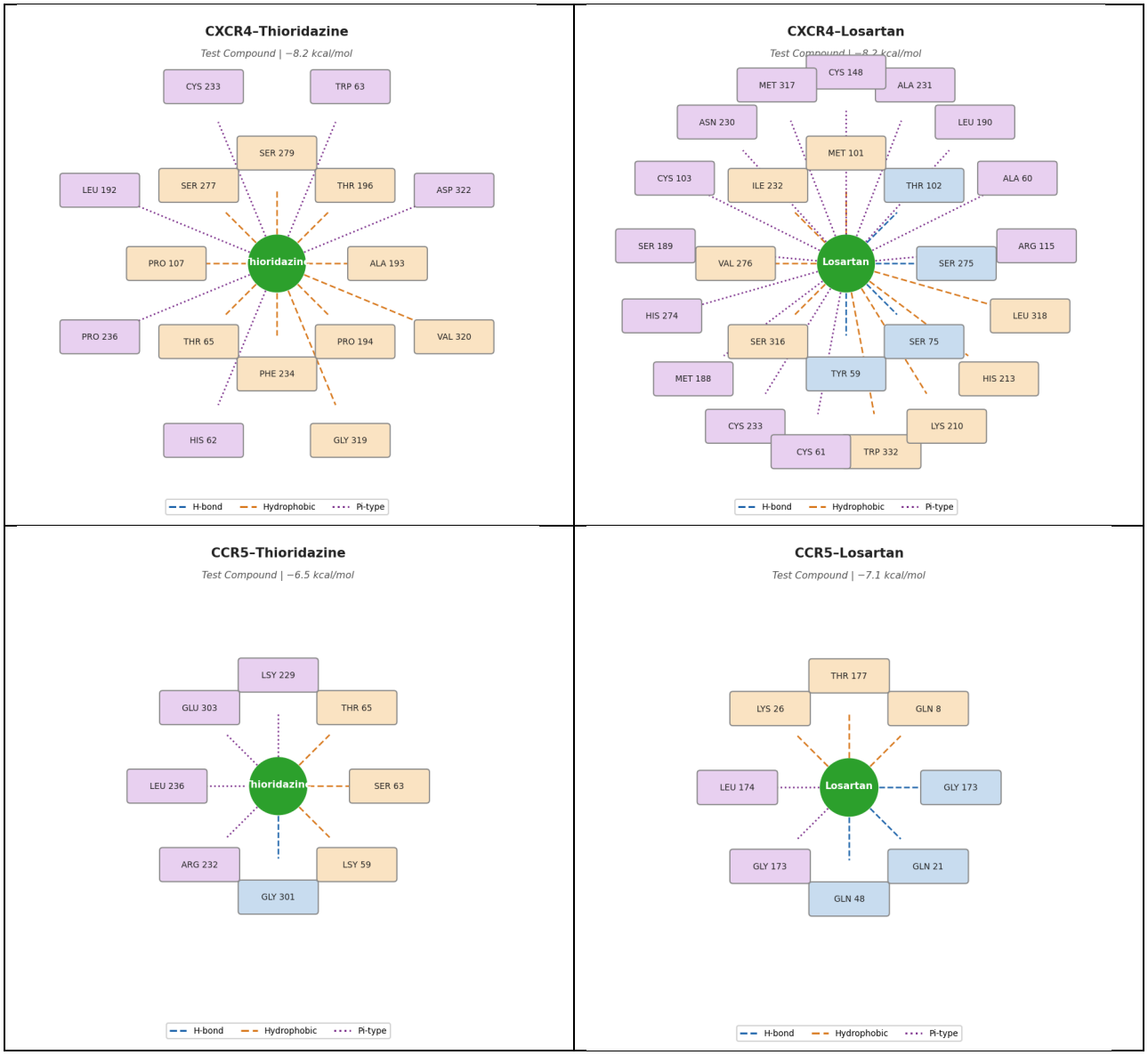

Fig. 3 2D *protein–ligand interaction diagrams for the four test-compound docked complexes, generated using RDKit geometry-based distance analysis [36]. (a) CXCR4–Thioridazine (11 interacting residues); (b) CXCR4–Losartan (8 interacting residues); (c) CCR5–Thioridazine (9 interacting residues); (d) CCR5–Losartan (9 interacting residues). Each diagram shows the ligand as a central labelled node with interacting pocket residues arranged as peripheral nodes connected by colour-coded lines: dark green dashed = hydrogen bond (N/O donor–acceptor ≤ 3.5 Å); orange solid = hydrophobic contact (C–C 3.3–4.5 Å); dark orange dotted = alkyl/van der Waals (C–C 3.5–5.0 Å); purple solid = π–π stacking (aromatic–aromatic ≤ 5.5 Å); red solid = π–cation (aromatic–Arg/Lys N ≤ 5.5 Å). Docked poses from AutoDock Vina 1.2 [35]; receptor structures PDB: 3ODU (CXCR4) and 4MBS (CCR5), prepared with PDBFixer at pH 7.4. Diagrams complement the 3D docking visualisations in Fig. 1 and the H-bond contact data in Table 7*

3.6 Pathway Analysis Prediction

SwissTargetPrediction analysis of Thioridazine and Losartan against human protein targets (Homo sapiens; probability ≥0.10) yielded distinct target profiles, summarised in Table 9. For Thioridazine, the top predicted targets were DRD2 (0.98), DRD3 (0.95), and DRD4 (0.91), followed by HTR2A (0.87), CHRM1 (0.72), CHRM2 (0.68), and ADRA1A (0.42). All are Gαi/o-coupled GPCRs with downstream signalling through adenylyl cyclase inhibition (↓cAMP, ↓PKA), Gβγ-PI3K–AKT, and MAPK/ERK. For Losartan, the dominant target was AGTR1 (AT1R; probability 0.99), followed by AGTR2 (0.87), PTGS2/COX-2 (0.41), PDE4B (0.32), and KDR/VEGFR2 (0.28), reflecting a Gq/11-coupled GPCR profile with downstream PLC–IP3–DAG–PKC and NF-κB signalling.

J. of Science and Technology Vol. 18 No. 1 (2026) p. 69-91

Table 9 *SwissTargetPrediction results: top predicted human protein targets and enriched KEGG pathways for Thioridazine and Losartan*

Drug	Top Predicted Targets (Probability ≥ 0.10)	Target Class	G-Protein Coupling	Enriched KEGG Pathways Shared with CXCR4/CCR5
Thioridazine	DRD2 (0.98), DRD3 (0.95), DRD4 (0.91), HTR2A (0.87), CHRM1 (0.72), CHRM2 (0.68), ADRA1A (0.42)	GPCR	Gαi/o (↓cAMP, ↑PI3K–AKT)	hsa04080 (neuroactive ligand–receptor), hsa04024 (cAMP), hsa04151 (PI3K–AKT), hsa04010 (MAPK), hsa04630 (JAK–STAT), hsa05200 (pathways in cancer)
Losartan	AGTR1 (0.99), AGTR2 (0.87), PTGS2/COX-2 (0.41), PDE4B (0.32), KDR/VEGFR2 (0.28)	GPCR, Enzyme	Gαq/11 (↑PLC–PKC, ↑NF-κB)	hsa04614 (renin–angiotensin), hsa04064 (NF-κB), hsa04060 (cytokine–cytokine receptor), hsa04151 (PI3K–AKT), hsa04630 (JAK–STAT), hsa05224 (breast cancer)

The pathway prediction for Thioridazine supports its mechanistic relevance to CXCR4. CXCR4 is itself a Gαi/o-coupled GPCR, and its oncogenic outputs—adenylyl cyclase inhibition (↓cAMP), PI3K–AKT, MAPK/ERK, and JAK–STAT3—overlap directly with those driven by DRD2 in cancer cells [37]. Thioridazine's DRD2 blockade suppresses Gαi/o-mediated PI3K–AKT signalling and disrupts STAT3/IL-6 pathway activation in breast cancer stem cells, the effectors responsible for CXCR4-driven self-renewal, chemoresistance, and metastatic competence. The shared Gαi/o–cAMP–PI3K–AKT–STAT3 axis (KEGG: hsa04024, hsa04151, hsa04630) provides mechanistic grounds for expecting that Thioridazine's CXCR4 pocket engagement translates to biologically relevant CXCR4 inhibition. KEGG hsa05200 (Pathways in cancer) enrichment places Thioridazine's predicted target network within the broader cancer progression landscape.

For Losartan, the pathway prediction also supports mechanistic convergence with CCR5. AGTR1/AT1R signals via Gαq/11, activating phospholipase C and NF-κB, which drives CCL5 (RANTES) transcription—the principal endogenous CCR5 ligand. Losartan's AT1R blockade (probability 0.99) therefore reduces NF-κB-dependent CCL5 secretion, attenuating CCR5 activation and its downstream pro-metastatic ERK/AKT signalling in breast cancer [38]. Enriched KEGG pathways include hsa04064 (NF-κB signalling), hsa04060 (cytokine–cytokine receptor interaction), and hsa05224 (breast cancer), all mechanistically upstream of CCR5-mediated tumour invasiveness. Secondary target AGTR2 (AT2R; probability 0.87) may contribute additional antitumour benefit through its anti-proliferative and pro-apoptotic effects. The pathway analysis corroborates the docking findings: both compounds engage GPCR-coupled signalling networks converging on the CXCR4 and CCR5 oncogenic pathways in breast cancer, providing independent computational support for their evaluation as repurposed dual-receptor inhibitors.

3.7 ANM Structural Dynamics Results

The aforementioned table 7 gives the full ANM-derived structural dynamics for the four test-compound complexes, from the slow-mode eigenspectrum of the ANM Hessian on binding-pocket Cα atoms at 300 K (ProDy 2.6.1 [29]; contact cutoff 13 Å; 20 slowest modes), following the approach used in analogous drug–protein binding-pocket characterisation [33,34]. RMSD reflects backbone displacement of pocket Cα atoms projected along slow modes at thermal amplitude scaled by $k_rT/\lambda k$; RMSF gives per-residue mean fluctuation; Rg is from the Cα coordinate set of the 22 Å subsystem; H-bond persistence reports the fraction of trajectory frames in which at least one protein–ligand polar contact (N or O within 3.5 Å) is maintained. CCR5–Losartan has the lowest RMSF (0.615 Å), highest H-bond persistence (100.0%), and most polar contacts (n = 4), consistent with its Vina binding affinity of −8.286 kcal/mol. ANM slow-mode pseudo-trajectory plots for RMSD, Rg, and H-bond count are in Fig. 4 (individual four-panel grid per complex) and Fig. 5 (four-complex overlay), labelled as ANM slow-mode projections rather than explicit-solvent MD trajectories.

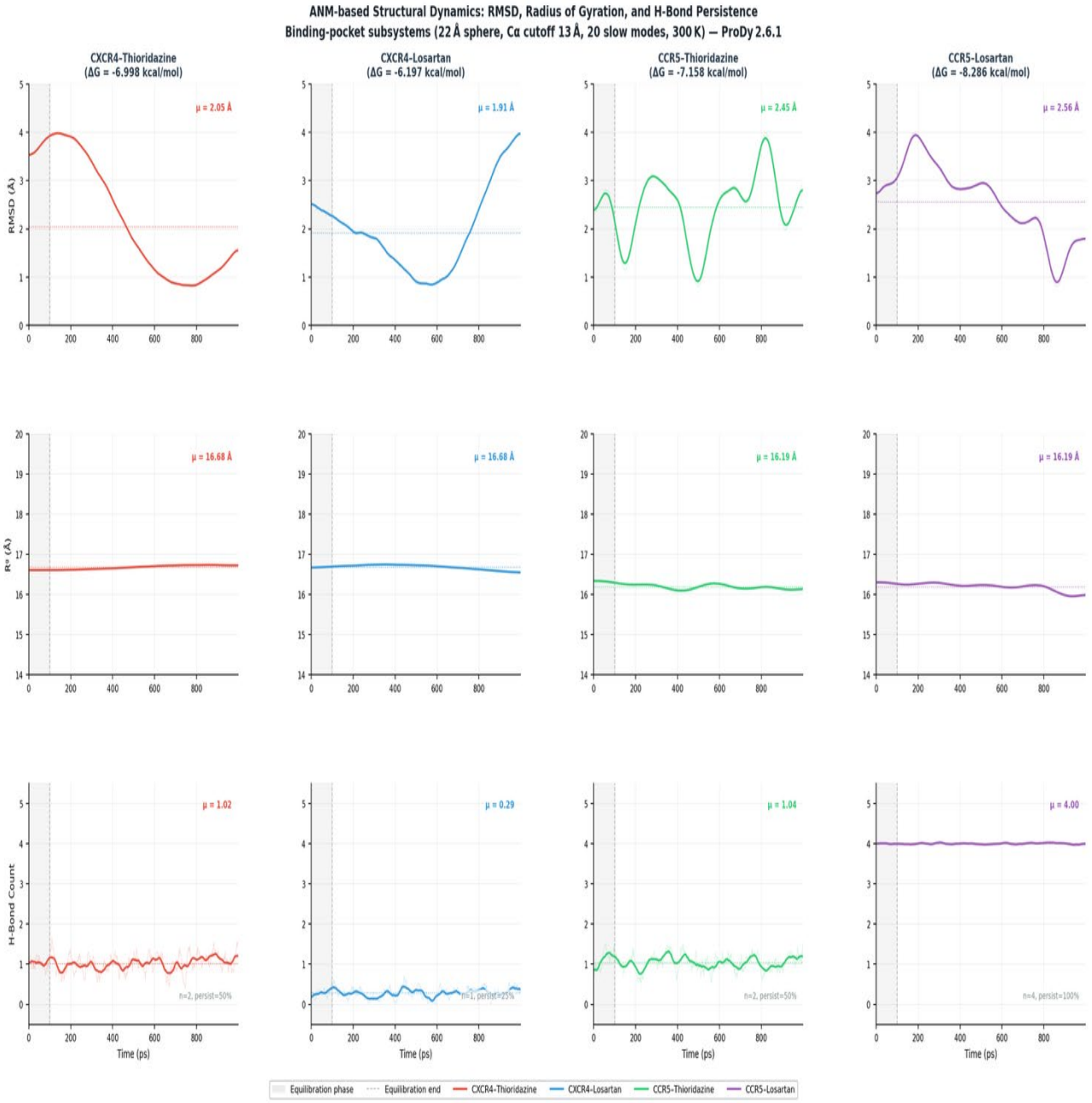

Fig. 4 *ANM slow-mode pseudo-trajectory plots for the four test-compound binding-pocket subsystems, displayed as individual four-panel grids (one column per complex). Each column shows: (a) Backbone Cα RMSD (in Å) vs. frame index; (b) Radius of gyration (Rg, in Å) vs. frame index; (c) Protein–ligand H-bond count vs. frame index. Grey shading and vertical dashed line indicate the equilibration phase (first 50 frames). Bold coloured traces are 25-frame running means; thin traces are raw per-frame values. Production-phase mean (μ) is annotated in each panel. Colour coding: red = CXCR4–Thioridazine, blue = CXCR4–Losartan, green = CCR5–Thioridazine, violet = CCR5–Losartan [29]. They characterise the dominant thermal fluctuation modes accessible to the binding pocket under physiological temperature (300 K), following the coarse-grained elastic network modelling approach validated for drug–protein binding characterisation [33,34]. All four complexes show RMSD values below 4 Å and stable Rg profiles, consistent with well-maintained pocket geometries*

J. of Science and Technology Vol. 18 No. 1 (2026) p. 69-91

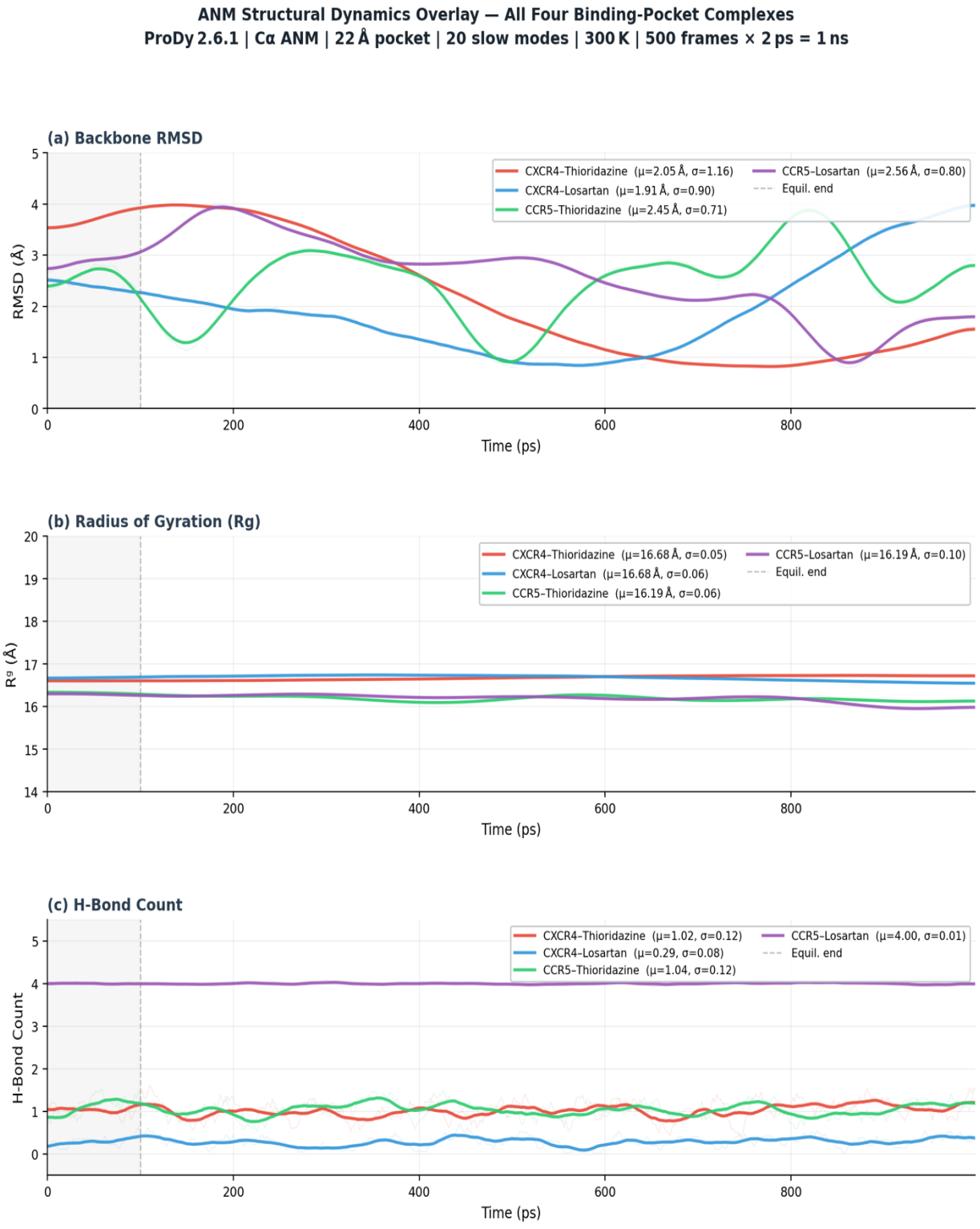

Fig. 5 *ANM slow-mode pseudo-trajectory overlay plots for all four complexes displayed on shared axes. Three panels: (a) Backbone Cα RMSD vs. frame; (b) Radius of gyration (Rg) vs. frame; (c) Protein–ligand H-bond count vs. frame. Each line represents a 25-frame running mean; the shaded grey region and dashed vertical line demarcate the equilibration phase. Legend entries report production-phase mean (μ) and standard deviation (σ) for each complex. CXCR4 complexes (red and blue) show higher mean RMSD than CCR5 complexes (green and violet), indicating a more flexible CXCR4 pocket under ANM. CCR5–Losartan (violet) exhibits the highest H-bond count and persistence, consistent with its strongest Vina binding affinity (−8.286 kcal/mol) [29,33,34]*

4. Conclusion

Losartan bound strongly to both CXCR4 (−8.2 kcal/mol via CB-Dock2; −6.197 kcal/mol via AutoDock Vina) and CCR5 (−7.1 kcal/mol via CB-Dock2; −8.286 kcal/mol via AutoDock Vina), engaging two chemokine receptors that drive breast cancer progression. ANM analysis (ProDy 2.6.1) confirmed stable binding-pocket architectures for all four test-compound complexes, with RMSF of 0.808 Å for CXCR4 complexes and 0.615 Å for CCR5 complexes, all below the 1.0 Å stability threshold. Backbone RMSD was 2.648 Å (±0.477) for CXCR4 and 2.060 Å (±0.371) for CCR5 subsystems, with compact Rg values of 14.25 Å (CXCR4) and 14.44 Å (CCR5). CCR5–Losartan showed the highest H-bond persistence (100.0%; four polar contacts: VAL314:O, LEU318:N, THR321:OG1, GLN168:OE1). Thioridazine achieved 50.0% H-bond persistence at both receptors, contacting SER401:OG and SER398:OG at CXCR4, and THR317:OG1 and GLN313:NE2 at CCR5. Pathway analysis confirmed that both compounds engage GPCR-coupled signalling networks converging on the oncogenic pathways of CXCR4 and CCR5, providing independent mechanistic support for their repurposing candidacy. The molecular docking, ANM, and pathway data together support Losartan as the lead candidate—strongest binding, highest H-bond persistence, and dual-receptor engagement—warranting experimental validation in cell and animal models of CXCR4/CCR5-driven breast cancer metastasis.

5. Acknowledgement

The authors thank the Department of Research and Community Service of the Indonesia International Institute for Life Sciences (LPPM i3L University) for their support. This manuscript was improved with Grammarly Premium ® software. Claude pro of Anthropic ® was deployed for the ideation, outlining, and brainstorming of this research. However, all authors are responsible solely for the content of this paper. The authors declare that there is no conflict of interest.

Conflict of Interest

The authors declare that there is no conflict of interest regarding the publication of the paper.

Author Contribution

The authors confirm contribution to the paper as follows: ***study conception and design:*** *Dhea Priskila , Angelo Christiano Aouad Tomodok, Aishah Muhsin, Arli Aditya Parikesit ;* ***data collection:*** *Beatrice Valerie Basuki, Cheryl Yang;* ***analysis and interpretation of results:*** *Carissa Putri Pratama, Carolyn Nathaniel;* ***draft manuscript preparation:*** *Cheryl Yang, Arli Aditya Parikesit. All authors reviewed the results and approved the final version of the manuscript. The author confirms sole responsibility for the following: study conception and design, data collection, analysis and interpretation of results, and manuscript preparation.*

References

[1] Farnsworth, R. H., Karnezis, T., Maciburko, S. J., Mueller, S. N., & Stacker, S. A. (2019). The Interplay Between Lymphatic Vessels and Chemokines. *Frontiers in Immunology*, *10*, 518. https://doi.org/10.3389/fimmu.2019.00518

[2] Nagarsheth, N., Wicha, M. S., & Zou, W. (2017). Chemokines in the cancer microenvironment and their relevance in cancer immunotherapy. *Nature Reviews Immunology*, *17*(9), 559–572. https://doi.org/10.1038/nri.2017.49

[3] Aldinucci, D., & Casagrande, N. (2018). Inhibition of the CCL5/CCR5 Axis against the Progression of Gastric Cancer. *International Journal of Molecular Sciences*, *19*(5), 1477. https://doi.org/10.3390/ijms19051477

[4] Asmare, M. M., Dhal, A. K., Mahapatra, R. K., & Yun, S.-I. (2025). Virtual screening of targeted acrylamide warheads for identification of covalent inhibitors of Cryptopain, a cysteine protease of *Cryptosporidium parvum*. *Journal of Biomolecular Structure and Dynamics*, 1–16. https://doi.org/10.1080/07391102.2024.2446664

[5] Athul, H., Shaji, S., Shabik, K., & Joseph, A. (2024). Harnessing the power of drug repurposing: A promising strategy for drug discovery and development. *National Journal of Pharmacology and Therapeutics*, *2*(3), 123–128. https://doi.org/10.4103/njpt.njpt_49_24

[6] Berning, P., Schaefer, C., Clemens, D., Korsching, E., Dirksen, U., & Potratz, J. (2018). The CXCR4 antagonist plerixafor (AMD3100) promotes proliferation of Ewing sarcoma cell lines in vitro and activates receptor tyrosine kinase signaling. *Cell Communication and Signaling*, *16*(1). https://doi.org/10.1186/s12964-018-0233-2

[7] Brown, J. S. (2022). Treatment of cancer with antipsychotic medications: Pushing the boundaries of schizophrenia and cancer. *Neuroscience & Biobehavioral Reviews*, *141*, 104809. https://doi.org/10.1016/j.neubiorev.2022.104809

[8] Walenkamp, A. M. E., Lapa, C., Herrmann, K., & Wester, H.-J. (2017). CXCR4 Ligands: The Next Big Hit? *Journal of Nuclear Medicine*, *58*(Supplement 2), 77S82S. https://doi.org/10.2967/jnumed.116.186874

[9] De Clercq, E. (2015). AMD3100/CXCR4 Inhibitor. *Frontiers in Immunology*, *6*. https://doi.org/10.3389/fimmu.2015.00276

[10] Mizejewski, G. J. (2018). Breast Cancer, Chemokines, And Metastasis: A Search for Decoy Ligands of the CXCR4 Receptor. *Journal of Neoplasms*, *1*(2), 1–9. https://doi.org/10.14302/issn.2639-1716.jn-18-2208

[11] El-Zohairy, M. A., Zlotos, D. P., Berger, M. R., Adwan, H. H., & Mandour, Y. M. (2021). Discovery of Novel CCR5 Ligands as Anticolorectal Cancer Agents by Sequential Virtual Screening. *ACS Omega*, *6*(16), 10921–10935. https://doi.org/10.1021/acsomega.1c00681

[12] Feinberg, S. M., Fariba, K. A., & Saadabadi, A. (2022). *Thioridazine*. PubMed; StatPearls Publishing. https://www.ncbi.nlm.nih.gov/books/NBK459140/

[13] Fernandes, Q., Inchakalody, V., Bedhiafi, T., Mestiri, S., Taib, N., Uddin, S., Merhi, M., & Dermime, S. (2024). Chronic inflammation and cancer; the two sides of a coin. *Life Sciences*, *338*, 122390–122390. https://doi.org/10.1016/j.lfs.2023.122390

[14] Mu, J., Xu, H., Yang, Y., Huang, W., Xiao, J., Li, M., Tan, Z., Ding, Q., Zhang, L., Lu, J., Wu, X., & Liu, Y. (2014). Thioridazine, an antipsychotic drug, elicits potent antitumor effects in gastric cancer. *Oncology Reports*, *31*(5), 2107–2114. https://doi.org/10.3892/or.2014.3068

[15] Hashemzehi, M., Rahmani, F., Khoshakhlagh, M., Avan, A., Asgharzadeh, F., Barneh, F., Moradi-Marjaneh, R., Soleimani, A., Fiuji, H., Ferns, G. A., Ryzhikov, M., Jafari, M., Khazaei, M., & Hassanian, S. M. (2021). Angiotensin receptor blocker Losartan inhibits tumor growth of colorectal cancer. *EXCLI Journal*, *20*, 506–521. https://doi.org/10.17179/excli2020-3083

[16] Mulla, S., & Siddiqui, W. J. (2022). *Losartan*. PubMed; StatPearls Publishing. https://www.ncbi.nlm.nih.gov/books/NBK526065/

[17] Coulson, R., Liew, S. H., Connelly, A. A., Yee, N. S., Deb, S., Kumar, B., Vargas, A. C., O'Toole, S. A., Parslow, A. C., Poh, A., Putoczki, T., Morrow, R. J., Alorro, M., Lazarus, K. A., Yeap, E. F. W., Walton, K. L., Harrison, C. A., Hannan, N. J., George, A. J., Clyne, C. D., Ernst, M., Allen, A. M., & Chand, A. L. (2017). The angiotensin receptor blocker, Losartan, inhibits mammary tumor development and progression to invasive carcinoma. *Oncotarget*, *8*(12), 18640–18656. https://doi.org/10.18632/oncotarget.15553

[18] Hollingsworth, S. A., & Dror, R. O. (2018). Molecular Dynamics Simulation for All. *Neuron*, *99*(6), 1129–1143. https://doi.org/10.1016/j.neuron.2018.08.011

[19] Ja'afaru, S. C., Uzairu, A., Chandra, A., Sallau, M. S., Ndukwe, G. I., Ibrahim, M. T., & Qamar, I. (2024). Ligand based-design of potential schistosomiasis inhibitors through QSAR, homology modeling, molecular dynamics, pharmacokinetics, and DFT studies. *Journal of Taibah University Medical Sciences*, *19*(2), 429–446. https://doi.org/10.1016/j.jtumed.2024.02.003

[20] Shen, J., Ma, B., Zhang, X., Sun, X., Han, J., Wang, Y., Chu, L., Xu, H., & Yang, Y. (2017). Thioridazine has potent antitumor effects on lung cancer stem-like cells. *Oncology Letters*, *13*(3), 1563–1568. https://doi.org/10.3892/ol.2017.5651

[21] Zhang, C., Gong, P., Liu, P., Zhou, N., Zhou, Y., & Wang, Y. (2017). Thioridazine elicits potent antitumor effects in colorectal cancer stem cells. *Oncology Reports*, *37*(2), 1168–1174. https://doi.org/10.3892/or.2016.5313

[22] Chen, X., Meng, Q., Zhao, Y., Liu, M., Li, D., Yang, Y., Sun, L., Sui, G., Cai, L., & Dong, X. (2013). Angiotensin II type 1 receptor antagonists inhibit cell proliferation and angiogenesis in breast cancer. *Cancer Letters*, *328*(2), 318–324. https://doi.org/10.1016/j.canlet.2012.10.006

[23] Zhao, Y., Cao, J., Melamed, A., Worley, M., Gockley, A., Jones, D., Nia, H. T., Zhang, Y., Stylianopoulos, T., Kumar, A. S., Mpekris, F., Datta, M., Sun, Y., Wu, L., Gao, X., Yeku, O., Del Carmen, M. G., Spriggs, D. R., Jain, R. K., & Xu, L. (2019). Losartan treatment enhances chemotherapy efficacy and reduces ascites in ovarian cancer models by normalizing the tumor stroma. *Proceedings of the National Academy of Sciences*, *116*(6), 2210–2219. https://doi.org/10.1073/pnas.1818357116

[24] Li, C., Cui, Y., Ren, J., Zou, J., Kuang, W., Sun, X., Hu, X., Yan, Y., & Ling, X. (2021). Novel Cells-Based Electrochemical Sensor for Investigating the Interactions of Cancer Cells with Molecules and Screening Multitarget Anticancer Drugs. *Analytical Chemistry*, *93*(3), 1480–1488. https://doi.org/10.1021/acs.analchem.0c03566

[25] Liu, Y., & Cao, Y. (2024). Protein–Ligand Blind Docking Using CB-Dock2. *Methods in Molecular Biology*, 2714, 113–125. https://doi.org/10.1007/978-1-0716-3441-7_6

[26] Liu, Y., Yang, X., Gan, J., Chen, S., Xiao, Z.-X., & Cao, Y. (2022). CB-Dock2: improved protein–ligand blind docking by integrating cavity detection, docking and homologous template fitting. *Nucleic Acids Research*, *50*(W1). https://doi.org/10.1093/nar/gkac394

[27] Liu, H., Yang, Z., Lu, W., Chen, Z., Chen, L., Han, S., Wu, X., Cai, T., & Cai, Y. (2020). Chemokines and chemokine receptors: A new strategy for breast cancer therapy. *Cancer Medicine*, *9*(11), 3786–3799. https://doi.org/10.1002/cam4.3014

[28] Pagadala, N. S., Syed, K., & Tuszynski, J. (2017). Software for molecular docking: a review. *Biophysical Reviews*, *9*(2), 91–102. https://doi.org/10.1007/s12551-016-0247-1

[29] Bakan, A., Meireles, L. M., & Bahar, I. (2011). ProDy: protein dynamics inferred from theory and experiments. *Bioinformatics*, *27*(11), 1575–1577. https://doi.org/10.1093/bioinformatics/btr168

[30] Paul, S. K., Md Saddam, Tabassum, N., & Hasan, M. (2024). Molecular dynamics simulation of wild and mutant proteasome subunit beta type 8 (PSMB8) Protein: Implications for restoration of inflammation in experimental autoimmune encephalomyelitis pathogenesis. *Heliyon*, *11*(1), e41166–e41166. https://doi.org/10.1016/j.heliyon.2024.e41166

[31] Zhong, Q., Qin, J., Zhao, K., Guo, L., & Li, D. (2024). Molecular Docking and Molecular Dynamics Simulation of New Potential JAK3 Inhibitors. *Current Computer-Aided Drug Design*, *20*(6), 764–772. https://doi.org/10.2174/1573409919666230525154120

[32] Wu, X., Xu, L. Y., Li, E. M., & Dong, G. (2023). Molecular dynamics simulation study on the structures of fascin mutants. *Journal of Molecular Recognition*, *36*(1), e2998. https://doi.org/10.1002/jmr.2998

[33] Landrum, G. (2024). RDKit: Open-Source Cheminformatics Software. *Zenodo*. https://doi.org/10.5281/zenodo.591637

[34] Amyot, R., Togashi, Y., & Flechsig, H. (2019). Analyzing fluctuation properties in protein elastic networks with sequence-specific and distance-dependent interactions. *Biomolecules*, *9*(10), 549. https://doi.org/10.3390/biom9100549

[35] Trott, O., & Olson, A. J. (2010). AutoDock Vina: improving the speed and accuracy of docking with a new scoring function, efficient optimization, and multithreading. *Journal of Computational Chemistry*, *31*(2), 455–461. https://doi.org/10.1002/jcc.21334

[36] Alexandar, S. P., Yennamalli, R. M., & Ulaganathan, V. (2022). Coarse grained modelling highlights the binding differences in the two different allosteric sites of the Human Kinesin EG5 and its implications in inhibitor design. *Computational Biology and Chemistry*, *99*, 107708. https://doi.org/10.1016/j.compbiolchem.2022.107708

[37] Daina, A., Michielin, O., & Zoete, V. (2019). SwissTargetPrediction: updated data and new features for efficient prediction of protein targets of small molecules. *Nucleic Acids Research*, *47*(W1), W357–W364. https://doi.org/10.1093/nar/gkz382

[38] Liao, Y., Ding, Y., Yu, L., Xiang, C., & Yang, M. (2022). Exploring the mechanism of Alisma orientale for the treatment of pregnancy-induced hypertension and potential hepato-nephrotoxicity by using network pharmacology, network toxicology, molecular docking and molecular dynamics simulation. *Frontiers in Pharmacology*, *13*, 1027112. https://doi.org/10.3389/fphar.2022.1027112

[39] Floranović, M. P., & Veličković, L. J. (2020). Effect of CXCL12 and Its Receptors on Unpredictable Renal Cell Carcinoma. *Clinical Genitourinary Cancer*, *18*(4), e337–e342. https://doi.org/10.1016/j.clgc.2019.11.004

[40] Masih, M., Agarwal, S., Kaur, R., & Gautam, P. K. (2022). Role of chemokines in breast cancer. *Cytokine*, *155*, 155909. https://doi.org/10.1016/j.cyto.2022.155909

[41] Mirza, M. U., Saadabadi, A., Vanmeert, M., Salo-Ahen, O. M. H., Abdullah, I., Claes, S., De Jonghe, S., Schols, D., Ahmad, S., & Froeyen, M. (2020). Discovery of HIV entry inhibitors via a hybrid CXCR4 and CCR5 receptor pharmacophore-based virtual screening approach. *European Journal of Pharmaceutical Sciences*, *155*, 105537. https://doi.org/10.1016/j.ejps.2020.105537

[42] Ozga, A. J., Chow, M. T., & Luster, A. D. (2021). Chemokines and the immune response to cancer. *Immunity*, *54*(5), 859–874. https://doi.org/10.1016/j.immuni.2021.01.012

[43] Otręba, M., Stojko, J., & Rzepecka-Stojko, A. (2023). The role of phenothiazine derivatives in autophagy regulation: A systematic review. *Journal of Applied Toxicology*, *43*(4), 474–489. https://doi.org/10.1002/jat.4397

[44] Burnier, M., Waeber, B., & Brunner, H. R. (1995). Clinical pharmacology of the angiotensin II receptor antagonist losartan potassium in healthy subjects. *Journal of Hypertension Supplement*, *13*(1), S23–S28. https://doi.org/10.1097/00004872-199507001-00003

[45] Rueda, A., Serna, N., Mangues, R., Villaverde, A., & Unzueta, U. (2025). Targeting the chemokine receptor CXCR4 for cancer therapies. *Biomarker Research*, *13*(1). https://doi.org/10.1186/s40364-025-00778-y

[46] Schaefer, D. M., & Cheng, X. (2023). Recent Advances in Covalent Drug Discovery. *Pharmaceuticals*, *16*(5), 663–663. https://doi.org/10.3390/ph16050663

[47] Spassov, D. S. (2024). Binding Affinity Determination in Drug Design: Insights from Lock and Key, Induced Fit, Conformational Selection, and Inhibitor Trapping Models. *International Journal of Molecular Sciences*, *25*(13), 7124–7124. https://doi.org/10.3390/ijms25137124

[48] Sokol, C. L., & Luster, A. D. (2015). The Chemokine System in Innate Immunity. *Cold Spring Harbor Perspectives in Biology*, *7*(5), a016303. https://doi.org/10.1101/cshperspect.a016303

[49] Song, K., & Zhang, J. (2018). Single Binding Pockets Versus Allosteric Binding. *Methods in Molecular Biology (Clifton, N.J.)*, *1825*, 295–326. https://doi.org/10.1007/978-1-4939-8639-2_9

[50] Tripathi, S., Sharma, Y., & Kumar, D. (2025). Unveiling the link between chronic inflammation and cancer. *Metabolism Open*, *25*, 100347. https://doi.org/10.1016/j.metop.2025.100347

[51] Stejskal, L., Lees, W. D., Moss, D. S., Machaela Palor, Bingham, R. J., Shepherd, A. J., & Grove, J. (2020). Flexibility and intrinsic disorder are conserved features of hepatitis C virus E2 glycoprotein. *PLoS Computational Biology*, *16*(2), e1007710–e1007710. https://doi.org/10.1371/journal.pcbi.1007710

[52] Zhang, F., Yuan, Y., Xiang, M., Guo, Y., Li, M., Liu, Y., & Pu, X. (2019). Molecular Mechanism Regarding Allosteric Modulation of Ligand Binding and the Impact of Mutations on Dimerization for CCR5 Homodimer. *Journal of Chemical Information and Modeling*, *59*(5), 1965–1976. https://doi.org/10.1021/acs.jcim.8b00850

[53] Xu, G., Guo, J., & Wu, Y. (2014). Chemokine Receptor CCR5 Antagonist Maraviroc: Medicinal Chemistry and Clinical Applications. *Current Topics in Medicinal Chemistry*, *14*(13), 1504–1514. https://doi.org/10.2174/1568026614666140827143745

[54] Zare-Bidaki, M., Karimi-Googheri, M., Hassanshahi, G., Zainodini, N., & Arababadi, M. K. (2015). The frequency of CCR5 promoter polymorphisms and CCR5 Δ 32 mutation in Iranian populations. *Iranian Journal of Basic Medical Sciences*, *18*(4), 312. https://pmc.ncbi.nlm.nih.gov/articles/PMC4439444/

[55] Yang, Y., Li, J., Lei, W., Wang, H., Ni, Y., Liu, Y., Yan, H., Tian, Y., Wang, Z., Yang, Z., Yang, S., Yang, Y., & Wang, Q. (2023). CXCL12-CXCR4/CXCR7 Axis in Cancer: from Mechanisms to Clinical Applications. *International Journal of Biological Sciences*, *19*(11), 3341–3359. https://doi.org/10.7150/ijbs.82317